



1 **Modelling tree-ring cellulose $\delta^{18}\text{O}$ variations of two temperature-sensitive tree**
2 **species from North and South America**

3

4

5 **Authors:**

6 Aliénor Lavergne¹, Fabio Gennaretti¹, Camille Risi², Valérie Daux³, Etienne Boucher⁴, Martine
7 M. Savard⁵, Maud Naulier⁶, Ricardo Villalba⁷, Christian Bégin⁵ and Joël Guiot¹

8

9 ¹Aix Marseille Université, CNRS, IRD, Collège de France, CEREGE, ECCOREV, Aix-en-
10 Provence, France

11 ²Laboratoire de Météorologie Dynamique, IPSL, UPMC, CNRS, Paris, France

12 ³Laboratoire des Sciences du Climat et de l'Environnement, CEA-CNRS-UVSQ, 91191 Gif-sur-
13 Yvette, France

14 ⁴Department of Geography and GEOTOP, Université du Québec à Montréal, Montréal, Canada

15 ⁵Geological Survey of Canada, Natural Resources Canada, 490 rue de la Couronne, QC,
16 G1K9A9, Canada

17 ⁶Institut de Radioprotection et de Sûreté Nucléaire (IRSN), PRP-ENV, SERIS/LRTE, Saint-Paul-
18 lez-Durance, France

19 ⁷Instituto Argentino de Nivología, Glaciología y Ciencias Ambientales, IANIGLA-CONICET,
20 Mendoza, Argentina

21

22 **Corresponding authors:** Aliénor Lavergne (alienor.lavergne@gmail.com) and Fabio Gennaretti
23 (gennaretti@cerege.fr)

24 Tel : +33 (0) 4 42 97 15 32

25 Centre Européen de Recherche et d'Enseignement en Géosciences

26 Technopôle de l'Arbois-Méditerranée

27 13545 Aix-en-Provence, FRANCE

28



29 **ABSTRACT**

30 Oxygen isotopes in tree-rings ($\delta^{18}\text{O}_{\text{TR}}$) are widely used to reconstruct past climates. However, the
31 complexity of climatic and biological processes controlling isotopic fractionation is not yet fully
32 understood. Here, we use the MAIDENiso model to decipher the variability of $\delta^{18}\text{O}_{\text{TR}}$ of two
33 temperature-sensitive species of relevant paleoclimatological interest (*Picea mariana* and
34 *Nothofagus pumilio*) and growing at cold high-latitudes in North and South America. In this first
35 modelling study on $\delta^{18}\text{O}_{\text{TR}}$ values in both northeastern Canada (53.86°N) and western Argentina
36 (41.10°S), we specifically aim at: 1) evaluating the predictive skill of MAIDENiso to simulate
37 $\delta^{18}\text{O}_{\text{TR}}$ values, 2) identifying the physical processes controlling $\delta^{18}\text{O}_{\text{TR}}$ by mechanistic modelling
38 and, 3) defining the origin of the temperature signal recorded in the two species. Although the
39 linear regression models used here to predict daily $\delta^{18}\text{O}$ of precipitation ($\delta^{18}\text{O}_{\text{P}}$) may need to be
40 improved in the future, the resulting daily $\delta^{18}\text{O}_{\text{P}}$ values adequately reproduce observed (from
41 weather stations) and simulated (by global circulation model) $\delta^{18}\text{O}_{\text{P}}$ series. The $\delta^{18}\text{O}_{\text{TR}}$ values of
42 the two species are correctly simulated using the $\delta^{18}\text{O}_{\text{P}}$ estimation as MAIDENiso input, although
43 some offset in mean $\delta^{18}\text{O}_{\text{TR}}$ levels is observed for the South American site. For both species, the
44 variability of $\delta^{18}\text{O}_{\text{TR}}$ series is more likely linked to the effect of temperature on isotopic
45 enrichment of the leaf water rather than on the isotopic composition of the source water. We
46 show that MAIDENiso is a powerful tool for investigating isotopic fractionation processes but
47 that the lack of a denser isotope-enabled monitoring network recording oxygen fractionation in
48 the soil-vegetation-atmosphere compartments limits our capacity to decipher the processes at
49 play. This study proves that the eco-physiological modelling of $\delta^{18}\text{O}_{\text{TR}}$ values is necessary to
50 interpret the recorded climate signal more reliably.

51

52 **Keywords:** MAIDENiso model, $\delta^{18}\text{O}$, tree-ring, *Nothofagus pumilio*, *Picea mariana*

53

54

55



56 1. INTRODUCTION

57 Oxygen isotopes in tree rings ($\delta^{18}\text{O}_{\text{TR}}$) are increasingly used as indicators of past climatic
58 changes in temperate areas (Cernusak and English, 2015; Hartl-Meier et al., 2014; Saurer et al.,
59 2008). They have been widely used to reconstruct past atmospheric conditions such as air
60 temperature (Naulier et al., 2015), drought (Labuhn et al., 2016), precipitation amount (Rinne et
61 al., 2013), isotopic composition of precipitation (Danis et al., 2006), relative air humidity
62 (Wernicke et al., 2015), cloud cover (Shi et al., 2012), and even atmospheric circulation patterns
63 (Brienen et al., 2012). This diversity of climatic targets possibly reconstructed based on oxygen
64 isotopes hints at the challenge of understanding the complexity of the climatic and biological
65 processes that control isotopic fractionation of oxygen in trees (Treydte et al., 2014).
66 Uncertainties arise because different poorly measured factors influence $\delta^{18}\text{O}_{\text{TR}}$ values. Isotopic
67 signals in tree-rings cellulose are strongly influenced by isotopic signature of soil water taken up
68 by the roots and by evaporative and physiological processes occurring at the leaf level and during
69 downstream metabolism (Barbour et al., 2005; Gessler et al., 2014). Thus, a comprehensive
70 approach that embraces existing mechanistic understanding of the fractionation processes
71 involved is required.

72

73 Few isotopic process-based models have been developed to investigate the mechanistic rules
74 governing the $\delta^{18}\text{O}_{\text{TR}}$ variations (Guiot et al., 2014): the Péclet-modified Craig-Gordon model
75 (Kahmen et al., 2011) and the Roden's model (Roden et al., 2000) are able to estimate, at a daily
76 time step, the $\delta^{18}\text{O}$ values of soil and xylem waters, and the isotopic fractionation occurring in the
77 leaves due to evapotranspiration. Versions of these models are integrated in more complete forest
78 ecophysiological models simulating the ensemble of forest water and carbon fluxes: (1)
79 MAIDEN (Modeling and Analysis In DENdroecology) (Gea-Izquierdo et al., 2015; Misson,
80 2004), which contains the isotopic module MAIDENiso (Danis et al., 2012) and (2) MUSICA
81 (Ogée et al., 2003, 2009). Both are accounting for important post-photosynthetic factors and are
82 able to link photosynthesis and carbohydrate allocation to stem growth.

83

84 In this paper, we use the MAIDENiso model to decipher the $\delta^{18}\text{O}_{\text{TR}}$ variability in American
85 temperature-sensitive species (*Picea mariana* in northeastern Canada and *Nothofagus pumilio* in
86 western Argentina). The selected sites are of special interest for paleoclimatology given that their



87 $\delta^{18}\text{O}_{\text{TR}}$ chronologies carry strong temperature signals. A summer temperature reconstruction was
88 already developed at the North American site (Gennaretti et al., 2017a; Naulier et al., 2015) and a
89 calibration study conducted at the South American one highlighted the strong potential of $\delta^{18}\text{O}_{\text{TR}}$
90 values to reflect variations in summer-autumn temperatures over a large region south of 38°S
91 (Lavergne et al., 2016). However, up to now, the climate- $\delta^{18}\text{O}_{\text{TR}}$ relationships were analysed
92 using a black box approach based on linear models. Here, we specifically aim at: 1) evaluating
93 the predictive skill of MAIDENiso to simulate $\delta^{18}\text{O}_{\text{TR}}$ values, 2) identifying the physical
94 processes controlling $\delta^{18}\text{O}_{\text{TR}}$ by mechanistic modelling and, 3) defining the origin of the
95 temperature signal recorded in the two species.

96

97 2. DATA AND METHODS

98 2.1. Sampling sites and tree-ring data

99 Two high-latitude American native species were studied here: 1) *Picea mariana* (Mill. B.S.P.;
100 black spruce), which is a conifer widely distributed over the American boreal forest (Viereck and
101 Johnston, 1990); and 2) *Nothofagus pumilio* (Poepp. et Endl. Krasser; lenga), which is a
102 deciduous species dominating the high-elevation forests along the Patagonian Andes from 35°S
103 to 55°S (Donoso, 1981; Schlatter, 1994). We selected two sites of *P. mariana* in the centre of the
104 Quebec-Labrador Peninsula in northeastern Canada (L01 and L20; from 53°51'N-72°24'W to
105 54°33'N-71°14'W, ~480 m elevation; see Gennaretti et al. (2014) and Naulier et al. (2014) for
106 details) and three sites of *N. pumilio* in northern Patagonia, western Argentina (NUB, ALM and
107 CHA; from 41°09'S-71°48'W to 41°15'S-71°17'W, 1270-1610 m elevation; see Lavergne et al.
108 (2016, 2017) for details). Climate in northeastern Canada is mostly continental and subarctic with
109 short, mild and wet summers and long, cold and dry winter. Total annual precipitation averages
110 825 mm with up to 46% falling during the growing season in summer (June to September)
111 (Naulier et al., 2014). In western Argentina, precipitation is largely concentrated from late fall to
112 early spring followed by a drier and mild period during summer and early fall (López Bernal et
113 al., 2012).

114

115 Four trees per site were collected for both species. The selection of the samples and analytical
116 procedure for $\delta^{18}\text{O}_{\text{TR}}$ measurements were described in Lavergne et al. (2016) and Naulier et al.



117 (2014). The developed $\delta^{18}\text{O}_{\text{TR}}$ chronologies covered the 1950-2005 and 1952-2011 periods at the
118 northeastern Canadian and western Argentinian sites, respectively. For each species, the
119 chronologies obtained at the different stands being significantly inter-correlated (Figure 1), we
120 chose to combine them and to develop one isotopic chronology for each of the two species.

121

122 **2.2. Modelling oxygen isotopes in tree-ring cellulose with MAIDENiso**

123 MAIDENiso is a process-based model that can simulate in parallel phenological and
124 meteorological controls on photosynthetic activity and carbon allocation. It explicitly allocates
125 carbohydrates to different carbon pools (leaves, stem, storage and roots) on a daily basis using
126 phenological stage-dependent rules. It also simulates the fractionation of carbon and oxygen
127 isotopes during growth processes. In particular, it estimates at a daily time step $\delta^{18}\text{O}$ values of
128 soil water and xylem water, the isotopic fractionation occurring in the leaves due to
129 evapotranspiration and the biochemical fractionation during cellulose formation. It uses as input
130 daily maximum and minimum temperature ($^{\circ}\text{C}$), precipitation (cm/day), atmospheric CO_2
131 concentration (ppm) and $\delta^{18}\text{O}$ values of precipitation ($\delta^{18}\text{O}_{\text{P}}$ in ‰).

132

133 In this study, the calculation of the daily $\delta^{18}\text{O}_{\text{TR}}$ in tree-ring cellulose (‰) is based on the (Danis
134 et al., 2012)'s formulation of the Craig-Gordon model (Craig and Gordon, 1965):

$$135 \quad \delta^{18}\text{O}_{\text{TR}} = (1-f_o) \cdot [\varepsilon^* + \varepsilon_k \cdot (1-h_{\text{air}}) + h_{\text{air}} \cdot \delta^{18}\text{O}_{\text{V}} + (1-h_{\text{air}}) \cdot \delta^{18}\text{O}_{\text{XW}}] + f_o \cdot \delta^{18}\text{O}_{\text{XW}} + \varepsilon_0 \quad (1)$$

136 This equation summarizes how $\delta^{18}\text{O}_{\text{TR}}$ is determined by:

- 137 (i) the $\delta^{18}\text{O}$ of the source (xylem) water ($\delta^{18}\text{O}_{\text{XW}}$), which is computed by averaging the
138 $\delta^{18}\text{O}_{\text{SW}}$ values of the different soil layers weighted by the volume of water taken up by
139 the roots in each layer. The isotopic effects of water mixing and soil evaporation on
140 the $\delta^{18}\text{O}_{\text{SW}}$ values of the different soil layers are computed by a mass and isotopic
141 balance (Danis et al., 2012). It is worth noting that no fractionation occurs during
142 water uptake by roots (Wershaw et al., 1966), neither during the transport of water
143 from the roots to the leaves.
- 144 (ii) the ^{18}O enrichment of the leaf water due to transpiration is described by
145 $(\varepsilon^* + \varepsilon_k \cdot (1-h_{\text{air}}) + h_{\text{air}} \cdot \delta^{18}\text{O}_{\text{V}} + (1-h_{\text{air}}) \cdot \delta^{18}\text{O}_{\text{XW}})$ after (Craig and Gordon, 1965), where:



- 146 a. ϵ^* is the equilibrium fractionation due to the change of phase from liquid water to
147 vapour at the leaf temperature (fixed at 21.4°C, the temperature threshold for
148 maximum carbon assimilation, ϵ^* is 9.65‰ (Helliker and Richter, 2008)),
149 b. ϵ_k is the kinetic fractionation due to the diffusion of vapour into unsaturated air
150 through the stomata and the leaf boundary layer,
151 c. h_{air} is the relative humidity of the evaporating air mass estimated from daily air
152 temperature (T_{air} ; °C; mean of the maximum and minimum air temperatures), and
153 the dew point temperature (T_r ; °C) (Running et al., 1987),
154 d. $\delta^{18}\text{O}_V$ is the atmospheric water vapour calculated assuming a precipitation-vapour
155 isotopic equilibrium (see below);
156 (iii) the biochemical fractionations (ϵ_0) due to oxygen exchange between carbonyl groups
157 (C = O) in the organic molecules and water (DeNiro and Epstein, 1979; Farquhar et
158 al., 1998).
159 (iv) the dampening factor f_o reflecting the exchange of the oxygen atoms between sucrose
160 and xylem water during cellulose synthesis in the xylem cells of tree rings.

161 As previously evoked (i), $\delta^{18}\text{O}_{\text{XW}}$ of Eq. 1 depends on $\delta^{18}\text{O}_{\text{SW}}$ and thus on $\delta^{18}\text{O}_P$ values. However,
162 long continuous time series of $\delta^{18}\text{O}_P$ are not available in the studied area. Here, we tested the
163 impact of using two different methods for deriving $\delta^{18}\text{O}_P$ time series.

164 Firstly, a linear model was used to estimate the daily values of $\delta^{18}\text{O}_P$ and subsequently $\delta^{18}\text{O}_V$
165 based on the primary drivers of their temporal variability (Dansgaard, 1964; Horita and
166 Wesolowski, 1994), that are air temperature (T_{air} ; °C) and precipitation at the corresponding site
167 (P; mm):

$$168 \quad \delta^{18}\text{O}_P = a \cdot T_{\text{air}} + b \cdot P + c \quad (2)$$

$$169 \quad \delta^{18}\text{O}_V = \delta^{18}\text{O}_P - \epsilon^*_{T_{\text{air}}} \quad (3)$$

170 with $\epsilon^*_{T_{\text{air}}}$ the fractionation due to the change of phase from liquid water to vapour at the mean air
171 temperature. The coefficients a and b were allowed to vary over a plausible range (or prior range)
172 in the calibration process together with other MAIDENiso parameters, while coefficient c was
173 fixed to a likely value (see Table 1 and section 2.4). This estimated set of data is referred in the
174 following as the estimated $\delta^{18}\text{O}_P$ dataset.



175 Secondly, we run the model with the series of the daily $\delta^{18}\text{O}_\text{P}$ derived from two general
176 circulation models (GCM) with different spatial resolutions and enough available data at our site
177 locations: 1) the MUGCM model (Noone and Simmonds, 2002) forced by varying sea surface
178 temperature (SST) from the HadISST data set for the 1950-2003 period ($2^\circ \times 2^\circ$ resolution;
179 extracted at <http://paos.colorado.edu/~dcn/SWING/database.php> ; hereafter referred as MUGCM
180 $\delta^{18}\text{O}_\text{P}$ dataset), and 2) the LMDZ5A model (Hourdin et al., 2013; Risi et al., 2010) with the
181 horizontal winds guided by those of the NCEP20 reanalysis for the 1950-2008 period (Compo et
182 al., 2011) ($2.5^\circ \times 3.75^\circ$ resolution; hereafter referred as LMDZ-NCEP20 $\delta^{18}\text{O}_\text{P}$ dataset).

183

184 The final $\delta^{18}\text{O}_\text{TR}$ time series are the annual average of the $\delta^{18}\text{O}_\text{TR}$ daily values (Eq. 1) weighted by
185 the daily simulated stand Gross Primary Production (GPP), assuming a proportional allocation of
186 carbon to the trunk. For the northeastern Canadian sites, the GPP simulated by MAIDENiso was
187 optimized using observations from an eddy covariance station (see Gennaretti et al. (2017a)).
188 Unfortunately, such observations were not available for *N. pumilio*, therefore the
189 parameterization obtained for the GPP of *P. mariana* was also used for the western Argentinian
190 sites but constraining the simulations with phenological observations extracted from the
191 literature. For example, to respect the annual cycle of the leaf area index (LAI) for *N. pumilio*
192 (Magnin et al., 2014; Rusch, 1993), we used in MAIDENiso a seasonal LAI annual cycle with a
193 development of leaves (LAI increase) between October and November, a maximum LAI (set at 5
194 leaf area/ground area) from November to April, a decreasing LAI (leaf fall) between April and
195 May, and finally a leafless period (null LAI) from June to September (Magnin et al., 2014;
196 Rusch, 1993). Furthermore, based on the finding that $\delta^{18}\text{O}_\text{TR}$ annual time series were more
197 correlated to climate variables of specific months of the growing season (Lavergne et al., 2016),
198 we also computed $\delta^{18}\text{O}_\text{TR}$ annual values by weighting the $\delta^{18}\text{O}_\text{TR}$ daily values (Eq. 1) with
199 synthetic GPP time series maximizing the correspondence between observations and simulations.

200

201 **2.3. Meteorological and atmospheric CO₂ data**

202 At the western Argentinian sites, we did not have long daily records of observed climate data.
203 Therefore, daily minimum–maximum temperature and precipitation data were derived from the
204 20th Century Reanalysis V2c (Compo et al., 2011) provided by the NOAA/OAR/ESRL ($2^\circ \times 2^\circ$
205 resolution, https://www.esrl.noaa.gov/psd/data/gridded/data.20thC_ReanV2c.html). The



206 temperature daily time series of the reanalysis were corrected in order to respect the monthly
207 mean values detected at Bariloche, the nearest meteorological station from our sampling sites
208 (~48 km from the sites, 41°12' S–71°12' W, 840 m asl; Servicio Meteorológico Nacional,
209 Argentina). The resulting maximum and minimum temperature series, covering the 1952-2011
210 period, fit well with the daily local temperature data from La Almohadilla (ALM) site (41°11'S,
211 71°47'W, 1410 m asl; data measured by dataloggers and provided by IANIGLA) available over
212 the 2002-2012 period ($r = 0.74$, $p < 0.001$; Figure SM1). For the northeastern Canadian sites,
213 climate data were obtained from the gridded interpolated Canadian database of daily minimum–
214 maximum temperature and precipitation covering the 1950-2005 studied period (0.08°×0.08°
215 resolution, (Hutchinson et al., 2009); <http://cfs.nrcan.gc.ca/projects/3/4>). In addition to these data
216 we also used for both the western Argentinian and northeastern Canadian sites modelled daily
217 data from the GCMs described above (see Table 2 with the input data used for each tested
218 configuration).

219

220 Data on the atmospheric CO₂ concentration were derived from the Mauna Loa station over the
221 1958-2012 period (Keeling et al. (1976); <http://www.esrl.noaa.gov/gmd/ccgg/trends/>). For the
222 1950-1957 years, we extrapolated atmospheric CO₂ data using the trend and seasonal cycle
223 observed in the observations over the subsequent 10-years period (1958-1967).

224

225 **2.4. Estimation of parameters influencing $\delta^{18}\text{O}_{\text{TR}}$**

226 We used a Bayesian method for the simultaneous calibration of the various MAIDENiso
227 parameters specific to the study species and site. A set of 50 plausible blocks of parameters
228 (posterior values) was selected according to the method described in Gennaretti et al. (2017a)
229 using Markov Chain Monte Carlo (MCMC) sampling (Table 1). The following prior plausible
230 ranges were considered:

231 1) the prior ranges of the a and b coefficients in the equation of the daily $\delta^{18}\text{O}_{\text{P}}$ (Eq. 2) were
232 selected in order to get $\delta^{18}\text{O}_{\text{P}}$ values for each site consistent with the measured monthly local
233 values from the nearest stations of the Global Network of Isotopes in Precipitation (GNIP), and
234 with the simulated daily values from the LMDZ-NCEP20 model and from the MUGCM model
235 (see Table 1),



236 2) the range for the biochemical fractionation factor ϵ_0 was chosen between 24‰ and 30‰
237 (+27±3‰ after DeNiro and Epstein (1981); Sternberg (1989); Yakir and DeNiro (1990)),
238 3) the range for the kinetic fractionation ϵ_k , which has been set to 26.5‰ in Farquhar et al. (1989)
239 but that can vary over larger ranges (Buhay et al., 1996), was taken between 10‰ and 30‰ here,
240 4) the range for the dampening factor f_o was allowed to vary between 0.3 and 0.5 following
241 Saurer et al. (1997).

242

243 We tested the sensitivity of the MAIDENiso model to the calibrated parameters by modifying
244 them within their respective prior calibration range. To control the robustness of the calibrated
245 parameters, we performed the calibration of these parameters over two equal length intervals
246 (1950-1977 and 1978-2005 for *P. mariana*; 1952-1981 and 1982-2011 for *N. pumilio*) keeping
247 the second half for independent validation of the parameters estimates. Once the model was
248 calibrated for the two species, the MAIDENiso's performance to simulate *P. mariana* and *N.*
249 *pumilio* $\delta^{18}\text{O}_{\text{TR}}$ interannual data was evaluated using the correlation coefficients (r) and the root
250 mean square errors (RMSE) between observed and simulated values.

251

252 **2.5. Disentangling leaf-level fractionation processes and source water influences on** 253 **$\delta^{18}\text{O}_{\text{TR}}$ signature**

254 To define the relative contributions to the $\delta^{18}\text{O}_{\text{TR}}$ signature of the isotopic signal of the source
255 water (xylem water) and of the fractionation processes due to transpiration taking place in the
256 leaves, we designed two experimental simulations with MAIDENiso based on Eq. 1:

257 1) to quantify the influence of the variability of the isotopic composition of the xylem water
258 on $\delta^{18}\text{O}_{\text{TR}}$, we compared the reference simulations to those where the relative humidity
259 (h_{air}) and the isotopic composition of atmospheric vapour ($\delta^{18}\text{O}_{\text{V}}$) were assumed to be
260 constant. The constant values for h_{air} and $\delta^{18}\text{O}_{\text{V}}$ were defined as the averages of the
261 respective MAIDENiso outputs ($h_{\text{air}} = 0.62$ and 0.9 , and, $\delta^{18}\text{O}_{\text{V}} = -26.28\text{‰}$ and -17.34‰ ,
262 respectively for northeastern Canada and western Argentina; the XW_source experiment
263 simulation hereafter),

264 2) to quantify the influence of the isotopic enrichment of the leaf water due to transpiration
265 on $\delta^{18}\text{O}_{\text{TR}}$, we compared the reference simulations to those where the $\delta^{18}\text{O}_{\text{XW}}$ series were
266 assumed to be constant. The constant value for $\delta^{18}\text{O}_{\text{XW}}$ was estimated as the average of



267 the $\delta^{18}\text{O}_{\text{XW}}$ MAIDENiso outputs ($\delta^{18}\text{O}_{\text{XW}} = -13.81\text{‰}$ and -7.03‰ , respectively for
268 northeastern Canada and western Argentina; the Leaf_water_enrichment_driven
269 experiment simulation hereafter).

270 Comparison between the experimental and reference simulations (i.e. using the optimal values of
271 the parameters) was achieved through the calculation of the coefficient of determination (R^2).

272

273 3. RESULTS

274 3.1. Estimated versus modelled and observed $\delta^{18}\text{O}_\text{P}$ values

275 The modelled $\delta^{18}\text{O}_\text{P}$ series from the GCM models are similar to the GNIP datasets, with mean
276 values ranging from -12‰ to -8‰ over June-September in northeastern Canada (Figure SM2A)
277 and from -7‰ to -3‰ over December-April at the western Argentinian sites (Figure SM2B). In
278 general, $\delta^{18}\text{O}_\text{P}$ series from LMDZ-NCEP20 model in western Argentina are slightly displaced
279 toward higher values ($+1\text{‰}$) in comparison with the GNIP and MUGCM data. The estimated
280 $\delta^{18}\text{O}_\text{P}$ values based on plausible values of coefficients a and b agree well with those of the models
281 and observations in northeastern Canada. For the western Argentinian sites, they are 2-3‰ lower
282 from April to October, i.e. late spring-early autumn (Figure SM2).

283

284 3.2. Sensitivity of the model to the calibrated parameters

285 Most of the calibrated parameters have an influence on the correlations between observed and
286 simulated $\delta^{18}\text{O}_{\text{TR}}$ series and/or on the mean levels of the simulated series (Figure 2). The
287 temperature and precipitation dependences of $\delta^{18}\text{O}_\text{P}$ values (respectively a and b) have the
288 strongest influence on correlations. Increasing a and b values increase the mean $\delta^{18}\text{O}_{\text{TR}}$ levels,
289 most strongly in western Argentina than in northeastern Canada (Figure 2). Changes in the
290 dampening factor (f_0) and in the biochemical fractionation (ϵ_0) have almost no effect on
291 correlation, but their increase induces significant decrease of the mean levels of $\delta^{18}\text{O}_{\text{TR}}$ series.
292 Finally, increasing the kinetic fractionation (ϵ_k) leads to lower correlations and to higher mean
293 levels of $\delta^{18}\text{O}_{\text{TR}}$ (Figure 2).

294

295 3.3. MAIDENiso performance in reproducing observed $\delta^{18}\text{O}_{\text{TR}}$ series

296 Split-period verifications of the calibrated relationships for *P. mariana* and *N. pumilio* when
297 using estimated $\delta^{18}\text{O}_\text{P}$ series from Eq. 2 indicate that the calibration over either the first half or the



298 second half periods provide similar posterior densities of the calibrated parameters than the ones
299 obtained when calibrating over the whole periods (Figure SM3). One exception is observed in the
300 calibration of coefficient a in northeastern Canada over the two half periods, where the posterior
301 densities of a are different from the one obtained by calibrating over the entire period. Over the
302 entire periods, observed and simulated $\delta^{18}\text{O}_{\text{TR}}$ series are significantly correlated in northeastern
303 Canada ($r = 0.56$, $p < 0.01$ and $\text{RMSE} = 0.67$; Figure 3A) and in western Argentina ($r = 0.48$, $p <$
304 0.01 and $\text{RMSE} = 0.63$; Figure 3C). The correlation between observed and simulated $\delta^{18}\text{O}_{\text{TR}}$
305 series are slightly improved when we used synthetic daily GPP ($r = 0.62$ and $r = 0.52$, $p < 0.01$,
306 respectively for northeastern Canada and western Argentina; Figure 3B and 3D). It is worth
307 noting that the mean levels of the simulated $\delta^{18}\text{O}_{\text{TR}}$ series for the Argentinian sites are lower than
308 those of the observations (offset of around -2.5% ; Figure SM4). The series were therefore
309 corrected to respect the mean values detected in the observations (Figure 3C and 3D). In contrast,
310 the correlations between observation and simulation considerably decrease when we used
311 modelled $\delta^{18}\text{O}_{\text{P}}$ from MUGCM models or LMDZ-NCEP20 reanalysis data. They only reach
312 $r = 0.13$ ($p > 0.05$) to 0.23 ($p < 0.05$) in northeastern Canada and $r = 0.23$ to 0.26 ($p < 0.05$) in
313 western Argentina, respectively (Figure 4).

314

315 **3.4. Influence of source water and leaf water isotopic enrichment to the $\delta^{18}\text{O}_{\text{TR}}$ signature**

316 The relative contributions to the $\delta^{18}\text{O}_{\text{TR}}$ signature of the isotopic signal of the source (xylem)
317 water and of the ^{18}O enrichment of the leaf water due to transpiration were investigated. In both
318 regions, the Leaf_water_enrichment experimental simulations are more highly related to the
319 reference one (R^2 centred on 0.9 and 0.95 , respectively for northeastern Canada and western
320 Argentina; Figure 5) than the XW_source ones (R^2 centred on 0.65 and 0.8 , respectively for
321 northeastern Canada and western Argentina). This suggests that, with the model, the variability of
322 $\delta^{18}\text{O}_{\text{XW}}$ has a weaker influence on $\delta^{18}\text{O}_{\text{TR}}$ variations than the changes of the leaf water isotopic
323 enrichment do. Notably, *P. mariana* in northeastern Canada appears to be more sensitive to both
324 influences than *N. pumilio* in western Argentina (Figure 5). Caution should be made here since
325 these results are limited upstream by the performance of the regressions.

326

327



328 4. DISCUSSION

329 4.1. Precipitation $\delta^{18}\text{O}_P$ variations and estimation

330 Although the regression models used to predict daily $\delta^{18}\text{O}_P$ values are likely too simplistic, the
331 resultant monthly averaged values adequately reproduce the distribution of the observed (from
332 GNIP stations) and modelled (by GCMs) monthly $\delta^{18}\text{O}_P$ series in northeastern Canada. In
333 western Argentina, the distribution of monthly $\delta^{18}\text{O}_P$ values is also well reproduced but the
334 amplitude of variation of the predicted values is too high, leading to simulated values lower than
335 the measured ones during the colder months. The temporal $\delta^{18}\text{O}_P$ variations are positively related
336 to air temperature given the positive coefficient a . In agreement with the simple Rayleigh
337 distillation model (Dansgaard, 1964), as air temperature decreases, the specific humidity at
338 saturation decreases, and water vapour condenses. H_2^{18}O condenses preferentially, the residual
339 water vapour gets more and more depleted as condensation proceeds. In the Tropics, the relative
340 abundance of ^{18}O in the meteoric water has been observed to decrease with increasing amount of
341 precipitation and/or relative humidity leading to a decrease in $^{18}\text{O}/^{16}\text{O}$ ratio in a high amount of
342 precipitated water (Rozanski et al., 1993). In extra-tropical regions, $\delta^{18}\text{O}_P$ may also correlate with
343 precipitation amount (negative coefficient b), since both variables depend on the meteorological
344 conditions.

345 The results of the linear regressions show comparatively lower influence of precipitation on $\delta^{18}\text{O}_P$
346 in western Argentina than in northeastern Canada (Table 1). This suggests that the imprint of the
347 precipitation amount on $\delta^{18}\text{O}_P$ in western Argentina is low and that $\delta^{18}\text{O}_P$ variations are mainly
348 controlled by seasonal changes in temperature, which is in agreement with (Rozanski et al.,
349 1995). However, due to the strong west-to-east precipitation gradient in this region (orographic
350 rain shadow), large $\delta^{18}\text{O}_P$ variations occur over short distances (Rozanski et al., 1995; Smith and
351 Evans, 2007; Stern and Blisniuk, 2002). Therefore, the daily precipitation dataset extracted from
352 the gridded reanalysis data, which has a low spatial resolution (>200 km), may not represent the
353 daily variations in precipitation at a local scale faithfully. Therefore, the model may
354 underestimate the contribution of precipitation on $\delta^{18}\text{O}_P$ variability in this particular area.

355

356 Contrastingly, in northeastern Canada, both temperature and precipitation amount equally control
357 the $\delta^{18}\text{O}_P$ variations. The high amount of precipitation falling in summer ($\sim 46\%$) should have a
358 strong effect and decrease the $\delta^{18}\text{O}_P$ values in the condensed water, while high temperatures



359 counteract this effect by increasing this ratio. Before reaching northeastern Canada, the air
360 masses pushed by the dominant westerly winds discharge most of their humidity over the land,
361 leading to a depleted $\delta^{18}\text{O}_\text{P}$ signal at our sites (for the same reason, $\delta^{18}\text{O}_\text{TR}$ values at L20, which is
362 located 110 km North-East of L01, are $\sim 1\%$ lower). Interestingly, the $\delta^{18}\text{O}_\text{P}$ signal in
363 northeastern Canada is comparatively more depleted than in western Argentina. It is worth noting
364 that the resolution of the gridded meteorological dataset used here is relatively high (~ 10 km),
365 which means that the local processes are likely well represented.

366

367 **4.2. Relative performance in modelling $\delta^{18}\text{O}_\text{TR}$ values**

368 The simulated $\delta^{18}\text{O}_\text{TR}$ series based on daily $\delta^{18}\text{O}_\text{P}$ estimation from the regression models
369 reproduce the observations better than the ones based on $\delta^{18}\text{O}_\text{P}$ values derived from GCMs
370 (Figure 4). This is in part due to the greater number of parameters to optimize, as the calibration
371 process can more easily find a solution that fits the observations better. This may however reflect
372 error compensations especially in western Argentina where the estimated annual variability of
373 $\delta^{18}\text{O}_\text{P}$ is too large. Conversely in northeastern Canada, the annual variations of $\delta^{18}\text{O}_\text{P}$ that are
374 estimated, simulated by GCMs and observed are in good agreement (Figure SM2). Although
375 isotope-enabled atmospheric global models reproduce reasonably well the global distribution of
376 the mean annual isotope contents of the modern precipitation and their seasonality (Risi et al.,
377 2010), results at specific sites, especially in mountainous regions such as at our western
378 Argentinian site, can be less accurate (Figure SM2; see the offset between GNIP and LMDZ-
379 NCEP20). Ideally, daily $\delta^{18}\text{O}_\text{P}$ long-term records from meteorological stations in the study region
380 should be used as an input of MAIDENiso. Simulations from high-resolution regional circulation
381 models, such as REMOiso which has a $0.5^\circ \times 0.5^\circ$ (~ 55 km) horizontal resolution (Insel et al.,
382 2013; Sturm et al., 2007, 2005), may produce reliable local $\delta^{18}\text{O}_\text{P}$ values. Such dataset has proven
383 to be quite helpful with MAIDENiso in the Fontainebleau forest (France) (Danis et al., 2012).
384 However, up to now, measured or REMOiso $\delta^{18}\text{O}_\text{P}$ datasets in our regions of study do not exist,
385 which is the case for most regions of the world. Therefore, we recommend that daily GNIP
386 stations are set up in various forested ecosystems and that high resolution simulations of $\delta^{18}\text{O}_\text{P}$ are
387 performed in wider regions.

388



389 The modelling of $\delta^{18}\text{O}_{\text{TR}}$ values based on the estimation of $\delta^{18}\text{O}_{\text{P}}$ is relatively more accurate for
390 northeastern Canada than for western Argentina (Figure 3). As the mean levels of the measured
391 $\delta^{18}\text{O}_{\text{TR}}$ values are high at the western Argentinian sites (mean value of about 30‰), the Bayesian
392 optimization tends to increase the biochemical (ϵ_0) and kinetic (ϵ_k) fractionations as well as the
393 coefficient a , while reducing the dampening factor (f_0) to reach more representative mean levels
394 of the $\delta^{18}\text{O}_{\text{TR}}$ simulation. But still, these levels are too low in comparison with the observations
395 (about 2.5‰ lower; Figure SM4). When the posterior value of a calibrated parameter is limited to
396 the upper bound of the prior range of plausible values, as it is the case at the western Argentinian
397 sites for a , b and ϵ_0 (Figure SM3), it means that either the prior range is too narrow, or the model
398 is inadequate, or some important process is not considered in the model. Here, the estimation of
399 the prior ranges of both coefficients a and b were based on observed (GNIP stations) and
400 simulated (GCMs) $\delta^{18}\text{O}_{\text{P}}$ values. Therefore, we expect their respective ranges to be consistent
401 with local processes. When the prior range of a is extended to higher values in the optimization
402 process, observed and simulated $\delta^{18}\text{O}_{\text{TR}}$ mean levels in western Argentina are better matching.
403 However, in this case, the distribution of $\delta^{18}\text{O}_{\text{P}}$ values is shifted toward higher values, advocating
404 for unrealistic estimated $\delta^{18}\text{O}_{\text{P}}$ variations.

405 One other possibility is that the prior range of ϵ_0 is too narrow. In accordance with DeNiro and
406 Epstein (1981), Sternberg (1989) and Yakir and DeNiro (1990), the biochemical fractionation ϵ_0
407 is assumed here to be lower than 30‰. However, a recent study has demonstrated that this
408 parameter, nearly constant between 20 to 30°C, increases at lower temperatures to values of 31‰
409 (Sternberg and Ellsworth, 2011). During the growing season, maximum temperatures can reach
410 20°C in western Argentina and 30°C in northeastern Canada, which suggests that the high mean
411 $\delta^{18}\text{O}_{\text{TR}}$ levels in *N. pumilio* may be due to biochemical fractionation higher than 30‰ due to
412 temperature generally lower than 20°C. However, when the prior range of ϵ_0 is extended to 31‰
413 in the optimization process, the mean $\delta^{18}\text{O}_{\text{TR}}$ levels of *N. pumilio* are still too low in comparison
414 with the observations. These results advocate for the existence of other processes, which can
415 explain this offset in mean levels in Argentina. For example, higher soil water evaporation than
416 modelled by MAIDENiso should lead to less negative $\delta^{18}\text{O}_{\text{SW}}$ (and therefore $\delta^{18}\text{O}_{\text{XW}}$), which
417 could explain the high mean levels of $\delta^{18}\text{O}_{\text{TR}}$ in Argentina. Caution should be exercised with such
418 an interpretation since other species living in similar conditions as *N. pumilio* in western
419 Argentina show comparatively lower mean $\delta^{18}\text{O}_{\text{TR}}$ levels than *N. pumilio* (i.e., *Fitzroya*



420 *cupressoides*; see Lavergne et al. (2016)). The ongoing monitoring and evaluation of isotopic
421 processes based on synchronous measurements of vapour, precipitation, soil water and xylem
422 water will certainly help understanding the high mean levels observed in Argentina, and
423 increasing the representation of the involved processes in MAIDENiso.

424

425 The better fit between observed and simulated $\delta^{18}\text{O}_{\text{TR}}$ values obtained with specific forms of
426 synthetic distributions of daily GPP for northeastern Canada and western Argentina (Figure 3)
427 suggests differential limiting factors in the two regions. The synthetic bimodal distribution of
428 daily GPP with maxima in spring and autumn, as simulated in western Argentina, is often
429 observed in a diversity of ecosystems such as in the Mediterranean environments (Baldocchi et
430 al., 2010; Gea-Izquierdo et al., 2015). After the activation of the photosynthesis in early spring,
431 increasing temperatures tend to be optimal for tree growth. However, in a modelling study,
432 Lavergne et al. (2015) have shown that the influence of temperature on *N. pumilio*'s growth
433 becomes negative once a temperature threshold (soil moisture) is exceeded. Therefore, we
434 assume that after reaching a threshold of temperature and soil moisture summer conditions, tree
435 growth is not favoured, leading to a decrease of primary productivity. However, when
436 temperature starts to decline and soil water supply tends to increase with increasing precipitation
437 events, tree growth increases again until the end of the growing season. In contrast, because
438 precipitation is more abundant in summer (June to September) in northeastern Canada (Naulier et
439 al., 2014), high summer temperatures should be always beneficial to tree-growth if enough soil
440 water is available. Therefore, in agreement with GPP-derived eddy covariance data from the
441 Fluxnet network (see Gennaretti et al. (2017a)), a better fit between observations and simulations
442 is observed when using a unimodal rather than a bimodal GPP distribution. Monitoring of tree
443 physiology, environmental conditions and wood cell formation will provide a more detailed
444 representation of the complex biological and ecological processes operating in Patagonia,
445 allowing us to run the MAIDENiso model with better constraints.

446

447 **4.3. What is the main origin of the temperature signal recorded in $\delta^{18}\text{O}_{\text{TR}}$?**

448 The investigation of the relative contributions of the isotopic composition of the source (xylem)
449 water and of the ^{18}O enrichment of the leaf water by transpiration on the simulated $\delta^{18}\text{O}_{\text{TR}}$ reveals
450 that the variability of the former has a weaker influence on $\delta^{18}\text{O}_{\text{TR}}$ variations than that of the



451 latter in North and South America. Therefore, the temperature signal recorded in $\delta^{18}\text{O}_{\text{TR}}$ series
452 more likely reflects the effect of temperature on isotopic enrichment of the leaf water rather than
453 on the isotopic composition of the source water. At the leaf-level, air temperature has a strong
454 effect on the relative humidity and therefore on the vapour pressure deficit (VPD), i.e. the
455 difference between the saturation vapour pressure and the actual vapour pressure, which
456 modulates the transpiration (Barbour, 2007). Thus, the imprint of the ambient air temperature on
457 the fractionation processes occurring during transpiration is preferentially recorded in the tree-
458 rings of the two species. Furthermore, both the isotopic signature of the xylem water and of the
459 fractionation processes occurring at the evaporation sites of the leaves have comparatively higher
460 influence on $\delta^{18}\text{O}_{\text{TR}}$ in *P. mariana* than in *N. pumilio*. This is probably due to the lower amplitude
461 of the day-by-day variations of the relative humidity in western Argentina (SD = 5%) versus in
462 northeastern Canada (SD = 16%) that translates into a weaker influence of h_{air} variations and
463 therefore of leaf-level isotopic fractionation processes on $\delta^{18}\text{O}_{\text{TR}}$ values in western Argentina
464 than in northeastern Canada. These results highlight the potential of MAIDENiso model to better
465 refine the origin of the climatic signal recorded in the oxygen isotopic signature in the tree-rings
466 of different species.

467

468 5. CONCLUSION

469 Here, by using MAIDENiso model, we provided a mechanistic overview of the climatic and
470 biological processes controlling oxygen isotopic fractionation in two American temperature-
471 sensitive tree species. Firstly, we have shown that using regression-based rather than model-
472 based $\delta^{18}\text{O}_{\text{p}}$ estimates as inputs increases the predictive skills of our simulations, although this
473 may be at the price of error compensations. Secondly, our study reveals that the variability of the
474 isotopic composition of the source (xylem) water has a weaker influence on $\delta^{18}\text{O}_{\text{TR}}$ variations
475 than that of the ^{18}O enrichment of the leaf water by transpiration. Finally, these findings suggest
476 that the imprint of temperature recorded in $\delta^{18}\text{O}_{\text{TR}}$ of the two species is likely related to the effect
477 of temperature on isotopic enrichment of the leaf water. The isotopic monitoring of water within
478 the soil-vegetation-atmosphere compartments in future work will certainly provide the input and
479 control data necessary to better constrain MAIDENiso. Our study demonstrates that the eco-
480 physiological modelling of $\delta^{18}\text{O}_{\text{TR}}$ values is necessary and likely the only approach to accurately
481 interpret the recorded climate signal. Based on the calibrations of MAIDENiso presented here,



482 the next step involves inverse modelling approaches to perform paleoclimatic reconstructions in
483 North and South America that are less biased by the complex and nonlinear interactions between
484 climate, CO₂ concentrations and tree growth as recommended by Boucher et al. (2014).

485

486 **ACKNOWLEDGMENTS**

487 A.L. has been supported by a Research associate/Lecturer position at the Aix-Marseille
488 University (France). F.G. has received funding from the European Union's Horizon 2020
489 research and innovation program under the Marie Skłodowska-Curie grant agreement No
490 656896. We acknowledge all data providers: the Instituto Argentino de Nivología, Glaciología y
491 Ciencias Ambientales (IANIGLA, Argentina) for providing the daily temperature data from La
492 Almohadilla site; the National Meteorological Service from Argentina for providing the monthly
493 temperature data from Bariloche meteorological station (Argentina); the Department of Natural
494 Resources Canada for providing the daily climatic data used for Quebec; the US Department of
495 Energy, Office of Science Biological and Environmental Research (BER) and the National
496 Oceanic and Atmospheric Administration Climate Program Office for providing the daily
497 climatic data used for Argentina; and the SWING project for providing the daily $\delta^{18}\text{O}_p$ data from
498 MUGCM model.

499

500

References

- 501 Baldocchi, D. D., Ma, S., Rambal, S., Misson, L., Ourcival, J. M., Limousin, J. M., Pereira, J. and
502 Papale, D.: On the differential advantages of evergreenness and deciduousness in mediterranean
503 oak woodlands: A flux perspective, *Ecol. Appl.*, 20(6), 1583–1597, doi:10.1890/08-2047.1, 2010.
- 504 Barbour, M. M.: Stable oxygen isotope composition of plant tissue: a review, *Funct. Plant Biol.*,
505 34, 83–94, doi:10.1071/FP06228, 2007.
- 506 Barbour, M. M., Cernusak, L. A. and Farguhar, G. D.: Factors affecting the oxygen isotope ratio
507 of plant organic material, in *Stable Isotopes and Biosphere-Atmosphere Interactions: Processes*
508 *and Biological Controls*, edited by L. B. Flanagan, J. R. Ehleringer, and D. E. Pataki, pp. 9–28,
509 Elsevier, Amsterdam., 2005.
- 510 Boucher, E., Guiot, J., Hatté, C., Daux, V., Danis, P. A. and Dussouillez, P.: An inverse modeling
511 approach for tree-ring-based climate reconstructions under changing atmospheric CO₂
512 concentrations, *Biogeosciences*, 11(12), 3245–3258, doi:10.5194/bgd-10-18479-2013, 2014.



- 513 Brienen, R. J. W., Helle, G., Pons, T. L., Guyot, J.-L. and Gloor, M.: Oxygen isotopes in tree
514 rings are a good proxy for Amazon precipitation and El Niño-Southern Oscillation variability,
515 *Proc. Natl. Acad. Sci.*, 109(42), 16957–16962, doi:10.1073/pnas.1205977109, 2012.
- 516 Buhay, W. M., Edwards, T. W. D. and Aravena, R.: Evaluating kinetic fractionation factors used
517 for reconstructions from oxygen and hydrogen isotope ratios in plant water and cellulose,
518 *Geochemistry, Geophys. Geosystems*, 60(12), 2209–2218, 1996.
- 519 Cernusak, L. A. and English, N. B.: Beyond tree-ring widths: stable isotopes sharpen the focus on
520 climate responses of temperate forest trees, *Tree Physiol.*, 35(1), 1–3,
521 doi:10.1093/treephys/tpu115, 2015.
- 522 Compo, G. P., Whitaker, J. S., Sardeshmukh, P. D., Matsui, N., Allan, R. J., Yin, X., Gleason, B.
523 E., Vose, R. S., Rutledge, G., Bessemoulin, P., BroNnimann, S., Brunet, M., Crouthamel, R. I.,
524 Grant, A. N., Groisman, P. Y., Jones, P. D., Kruk, M. C., Kruger, A. C., Marshall, G. J., Maugeri,
525 M., Mok, H. Y., Nordli, O., Ross, T. F., Trigo, R. M., Wang, X. L., Woodruff, S. D. and Worley,
526 S. J.: The Twentieth Century Reanalysis Project, *Q. J. R. Meteorol. Soc.*, 137(654), 1–28,
527 doi:10.1002/qj.776, 2011.
- 528 Craig, H. and Gordon, L. I.: Deuterium and oxygen 18 variations in the ocean and the marine
529 atmosphere, Spoleto., 1965.
- 530 Danis, P. A., Masson-Delmotte, V., Stievenard, M., Guillemin, M. T., Daux, V., Naveau, P. and
531 von Grafenstein, U.: Reconstruction of past precipitation $\delta^{18}\text{O}$ using tree-ring cellulose $\delta^{18}\text{O}$
532 and $\delta^{13}\text{C}$: A calibration study near Lac d'Annecy, France, *Earth Planet. Sci. Lett.*, 243(3–4),
533 439–448, doi:10.1016/j.epsl.2006.01.023, 2006.
- 534 Danis, P. A., Hatté, C., Misson, L. and Guiot, J.: MAIDENiso: a multiproxy biophysical model of
535 tree-ring width and oxygen and carbon isotopes, *Can. J. For. Res.*, 42(9), 1697–1713,
536 doi:10.1139/x2012-089, 2012.
- 537 Dansgaard, W.: Stable isotopes in precipitation, *Tellus A*, 16(4), 436–468,
538 doi:10.3402/tellusa.v16i4.8993, 1964.
- 539 DeNiro, M. J. and Epstein, S.: Relationship Between the Oxygen Isotope Ratios of Terrestrial,
540 *Science (80-.)*, 204, 6–8, 1979.
- 541 DeNiro, M. J. and Epstein, S.: Isotopic composition of cellulose from aquatic organisms,
542 *Geochim. Cosmochim. Acta*, 45(10), 1885–1894, doi:10.1016/0016-7037(81)90018-1, 1981.
- 543 Donoso, C.: Tipos forestales de los bosques nativos de Chile., Documento de Trabajo Nu. 38.



- 544 Investigación y Desarrollo Forestal (CONAF, PNUD-FAO). FAO Chile., 1981.
- 545 Farquhar, G. D., Hubick, H. T., Condon, A. G. and Richards, R. A.: Carbon isotope fractionation
546 and plant water-use efficiency, in *Stable Isotopes in Ecological Research*, pp. 21–40., 1989.
- 547 Farquhar, G. D., Barbour, M. M. and Henry, B. K.: Interpretation of oxygen isotope composition
548 of leaf material, in *Stable isotopes: integration of biological, ecological and geochemical*
549 *processes*, pp. 27–61, BIOS Scientific Publishers: Oxford., 1998.
- 550 Gea-Izquierdo, G., Guibal, F., Joffre, R., Ourcival, J. M., Simioni, G. and Guiot, J.: Modelling
551 the climatic drivers determining photosynthesis and carbon allocation in evergreen Mediterranean
552 forests using multiproxy long time series, *Biogeosciences*, 12(12), 3695–3712, doi:10.5194/bg-
553 12-3695-2015, 2015.
- 554 Gennaretti, F., Arseneault, D., Nicault, A., Perreault, L. and Bégin, Y.: Volcano-induced regime
555 shifts in millennial tree-ring chronologies from northeastern North America., *Proc. Natl. Acad.*
556 *Sci. U. S. A.*, (22), doi:10.1073/pnas.1324220111, 2014.
- 557 Gennaretti, F., Huard, D., Naulier, M., Savard, M., Bégin, C., Arseneault, D. and Guiot, J.:
558 Bayesian multiproxy temperature reconstruction with black spruce ring widths and stable
559 isotopes from the northern Quebec taiga, *Clim. Dyn.*, (123456789), 1–13, doi:10.1007/s00382-
560 017-3565-5, 2017a.
- 561 Gennaretti, F., Gea-Izquierdo, G., Boucher, E., Berninger, F., Arseneault, D. and Guiot, J.:
562 Ecophysiological modeling of the climate imprint on photosynthesis and carbon allocation to the
563 tree stem in the North American boreal forest, *Biogeosciences Discuss.*, (February), 1–26,
564 doi:10.5194/bg-2017-51, 2017b.
- 565 Gessler, A., Ferrio, J. P., Hommel, R., Treydte, K., Werner, R. A. and Monson, R. K.: Stable
566 isotopes in tree rings: towards a mechanistic understanding of isotope fractionation and mixing
567 processes from the leaves to the wood., *Tree Physiol.*, 0, 1–23, doi:10.1093/treephys/tpu040,
568 2014.
- 569 Guiot, J., Boucher, E. and Gea-Izquierdo, G.: Process models and model-data fusion in
570 dendroecology, *Front. Ecol. Evol.*, 2(August), 52, doi:10.3389/fevo.2014.00052, 2014.
- 571 Hartl-Meier, C., Zang, C., Büntgen, U. L. F., Esper, J. A. N., Rothe, A., Göttelein, A., Dirnböck,
572 T. and Treydte, K.: Uniform climate sensitivity in tree-ring stable isotopes across species and
573 sites in a mid-latitude temperate forest., *Tree Physiol.*, 2003(1), 4–15,
574 doi:10.1093/treephys/tpu096, 2014.



- 575 Helliker, B. R. and Richter, S. L.: Subtropical to boreal convergence of tree-leaf temperatures,
576 Nature, 454(7203), 511–514, doi:10.1038/nature07031, 2008.
- 577 Horita, J. and Wesolowski, D. J.: Liquid-vapor fractionation of oxygen and hydrogen isotopes of
578 water from the freezing to the critical temperature, Geochim. Cosmochim. Acta, 58(16), 3425–
579 3437, doi:10.1016/0016-7037(94)90096-5, 1994.
- 580 Hourdin, F., Grandpeix, J. Y., Rio, C., Bony, S., Jam, A., Cheruy, F., Rochetin, N., Fairhead, L.,
581 Idelkadi, A., Musat, I., Dufresne, J. L., Lahellec, A., Lefebvre, M. P. and Roehrig, R.: LMDZ5B:
582 The atmospheric component of the IPSL climate model with revisited parameterizations for
583 clouds and convection, Clim. Dyn., 40(9–10), 2193–2222, doi:10.1007/s00382-012-1343-y,
584 2013.
- 585 Hutchinson, M. F., McKenney, D. W., Lawrence, K., Pedlar, J. H., Hopkinson, R. F., Milewska,
586 E. and Papadopol, P.: Development and testing of Canada-wide interpolated spatial models of
587 daily minimum-maximum temperature and precipitation for 1961–2003, J. Appl. Meteorol.
588 Climatol., 48(4), 725–741, doi:10.1175/2008JAMC1979.1, 2009.
- 589 Insel, N., Poulsen, C. J., Sturm, C. and Ehlers, T. A.: Climate controls on Andean precipitation
590 $\delta^{18}\text{O}$ interannual variability, J. Geophys. Res. Atmos., 118(17), 9721–9742,
591 doi:10.1002/jgrd.50619, 2013.
- 592 Kahmen, A., Sachse, D., Arndt, S. K., Tu, K. P., Farrington, H., Vitousek, P. M. and Dawson, T.
593 E.: Cellulose $\delta^{18}\text{O}$ is an index of leaf-to-air vapor pressure difference (VPD) in tropical plants.,
594 Proc. Natl. Acad. Sci. U. S. A., 108(5), 1981–1986, doi:10.1073/pnas.1018906108, 2011.
- 595 Keeling, C. D., Bacastow, R. B., Bainbridge, A. E., Ekdahl Jr., C. . A., Guenther, P. R.,
596 Waterman, L. S. and Chin, J. F. S.: Atmospheric carbon dioxide variations at Mauna Loa
597 Observatory, Hawaii, Tellus A, 28, 538–551, doi:10.3402/tellusa.v28i6.11322, 1976.
- 598 Labuhn, I., Daux, V., Girardclos, O., Stievenard, M., Pierre, M. and Masson-Delmotte, V.:
599 French summer droughts since 1326 AD: a reconstruction based on tree ring cellulose $\delta^{18}\text{O}$,
600 Clim. Past, 11(6), 5113–5155, doi:10.5194/cpd-11-5113-2015, 2016.
- 601 Lavergne, A., Daux, V., Villalba, R. and Barichivich, J.: Temporal changes in climatic limitation
602 of tree-growth at upper treeline forests: Contrasted responses along the west-to-east humidity
603 gradient in Northern Patagonia, Dendrochronologia, 36, 49–59,
604 doi:10.1016/j.dendro.2015.09.001, 2015.
- 605 Lavergne, A., Daux, V., Villalba, R., Pierre, M., Stievenard, M., Srur, A. M. and Vimeux, F.: Are



606 the $\delta^{18}\text{O}$ of *F. cupressoides* and *N. pumilio* promising proxies for climate reconstructions in
607 northern Patagonia?, *J. Geophys. Res. - Biogeosciences*, 121(3), 767–776,
608 doi:10.1002/2015JG003260, 2016.

609 Lavergne, A., Daux, V., Villalba, R., Pierre, M., Stievenard, M. and Srur, A. M.: Improvement of
610 isotope-based climate reconstructions in Patagonia through a better understanding of climate
611 influences on isotopic fractionation in tree rings, *Earth Planet. Sci. Lett.*, 459, 372–380,
612 doi:10.1016/j.epsl.2016.11.045, 2017.

613 López Bernal, P., Defossé, G. E., Quinteros, C. P. and Bava, J. O.: Sustainable Management of
614 Lenga (*Nothofagus pumilio*) Forests Through Group Selection System, in *Sustainable Forest
615 Management - Current Research*, edited by D. J. J. D. (Ed.), pp. 45–66, InTech., 2012.

616 Magnin, A., Puntieri, J. and Villalba, R.: Interannual variations in primary and secondary growth
617 of *Nothofagus pumilio* and their relationships with climate, *Trees*, 28(5), 1463–1471, 2014.

618 Misson, L.: MAIDEN: a model for analyzing ecosystem processes in dendroecology, *Can. J. For.
619 Res.*, 34, 874–887, 2004.

620 Naulier, M., Savard, M. M., Bégin, C., Marion, J., Arseneault, D. and Bégin, Y.: Carbon and
621 oxygen isotopes of lakeshore black spruce trees in northeastern Canada as proxies for climatic
622 reconstruction, *Chem. Geol.*, 374–375, 37–43, doi:10.1016/j.chemgeo.2014.02.031, 2014.

623 Naulier, M., Savard, M. M., Bégin, C., Gennaretti, F., Arseneault, D., Marion, J., Nicault, A. and
624 Bégin, Y.: A millennial summer temperature reconstruction for northeastern Canada using
625 oxygen isotopes in subfossil trees, *Clim. Past*, 11(9), 1153–1164, doi:10.5194/cp-11-1153-2015,
626 2015.

627 Noone, D. and Simmonds, I.: Associations between $\delta^{18}\text{O}$ of water and climate parameters in a
628 simulation of atmospheric circulation for 1979–95, *J. Clim.*, 15, 3150–3169, 2002.

629 Ogée, J., Brunet, Y., Loustau, D., Berbigier, P. and Delzon, S.: MuSICA, a CO₂, water and
630 energy multilayer, multileaf pine forest model: Evaluation from hourly to yearly time scales and
631 sensitivity analysis, *Glob. Chang. Biol.*, 9(5), 697–717, doi:10.1046/j.1365-2486.2003.00628.x,
632 2003.

633 Ogée, J., Barbour, M. M., Wingate, L., Bert, D., Bosc, A., Stievenard, M., Lambrot, C., Pierre,
634 M., Bariac, T., Loustau, D. and Dewar, R. C.: A single-substrate model to interpret intra-annual
635 stable isotope signals in tree-ring cellulose, *Plant, Cell Environ.*, 32(8), 1071–1090,
636 doi:10.1111/j.1365-3040.2009.01989.x, 2009.



- 637 Rinne, K. T., Loader, N. J., Switsur, V. R. and Waterhouse, J. S.: 400-year May-August
638 precipitation reconstruction for Southern England using oxygen isotopes in tree rings, *Quat. Sci.*
639 *Rev.*, 60, 13–25, doi:10.1016/j.quascirev.2012.10.048, 2013.
- 640 Risi, C., Bony, S., Vimeux, F. and Jouzel, J.: Water-stable isotopes in the LMDZ4 general
641 circulation model: Model evaluation for present-day and past climates and applications to
642 climatic interpretations of tropical isotopic records, *J. Geophys. Res. Atmos.*, 115(12), 1–27,
643 doi:10.1029/2009JD013255, 2010.
- 644 Roden, J. S., Lin, G. and Ehleringer, J. R.: A mechanistic model for interpretation of hydrogen
645 and oxygen isotope ratios in tree-ring cellulose, *Geochim. Cosmochim. Acta*, 64(1), 21–35,
646 doi:10.1016/S0016-7037(99)00195-7, 2000.
- 647 Rozanski, K., Araguás-Araguás, L. and Gonfiantini, R.: Isotopic Patterns in Modern Global
648 Precipitation, in *Climate Change in Continental Isotopic Records.*, edited by P. K. Swart, K. C.
649 Lohmann, J. McKenzie, and S. Savin, American Geophysical Union., 1993.
- 650 Rozanski, K., Araguás-Araguás, L. and Araguás, L. A.: Spatial and temporal variability of stable
651 isotope composition of precipitation over the South American continent, *Bull. l'Institut Fr.*
652 *d'études Andin.*, 24(3), 379–390, 1995.
- 653 Running, S. W., Nemani, R. R. and Hungerford, R. D.: Extrapolation of synoptic meteorological
654 data in mountainous terrain and its use for simulating forest evapotranspiration and
655 photosynthesis, *Can. J. For. Res.*, 17, 472–483, doi:10.1139/x87-081, 1987.
- 656 Rusch, V. E.: Altitudinal variation in the phenology of *Nothofagus pumilio* in Argentina, *Rev.*
657 *Chil. Hist. Nat.*, 66(2), 131–141, 1993.
- 658 Saurer, M., Aellen, K. and Siegwolf, R.: Correlating $\delta^{13}\text{C}$ and $\delta^{18}\text{O}$ in cellulose of trees, *Plant,*
659 *Cell Environ.*, 20, 1543–1550, doi:S, 1997.
- 660 Saurer, M., Cherubini, P., Reynolds-Henne, C. E., Treydte, K. S., Anderson, W. T. and Siegwolf,
661 R. T. W.: An investigation of the common signal in tree ring stable isotope chronologies at
662 temperate sites, *J. Geophys. Res. Biogeosciences*, 113(4), doi:10.1029/2008JG000689, 2008.
- 663 Schlatter, J.: Requerimientos de sitio para la lenga, *Nothofagus pumilio* (Poepp. et Endl.) Krasser,
664 *Bosque*, 15, 3–10, 1994.
- 665 Shi, C., Daux, V., Zhang, Q. B., Risi, C., Hou, S. G., Stievenard, M., Pierre, M., Li, Z. and
666 Masson-Delmotte, V.: Reconstruction of southeast Tibetan Plateau summer climate using tree
667 ring $\delta^{18}\text{O}$: Moisture variability over the past two centuries, *Clim. Past*, 8(1), 205–213,



- 668 doi:10.5194/cp-8-205-2012, 2012.
- 669 Smith, R. B. and Evans, J. P.: Orographic Precipitation and Water Vapor Fractionation over the
670 Southern Andes, *J. Hydrometeorol.*, 8(1), 3–19, doi:10.1175/JHM555.1, 2007.
- 671 Stern, L. A. and Blisniuk, P. M.: Stable isotope composition of precipitation across the southern
672 Patagonian Andes, *J. Geophys. Res. Atmos.*, 107(23), doi:10.1029/2002JD002509p, 2002.
- 673 Sternberg, L. and Ellsworth, P. F. V.: Divergent biochemical fractionation, not convergent
674 temperature, explains cellulose oxygen isotope enrichment across latitudes, *PLoS One*, 6(11),
675 e28040, doi:10.1371/journal.pone.0028040, 2011.
- 676 Sternberg, L. D. S. L.: Oxygen and hydrogen isotope ratios in plant cellulose: Mechanisms and
677 applications, in *Stable Isotopes in Ecological Research*, edited by J. R. E. and K. A. N. P. W.
678 Rundel, pp. 124–141., 1989.
- 679 Sturm, C., Vimeux, F. and Krinner, G.: Intraseasonal variability in South America recorded in
680 stable water isotopes, *J. Geophys. Res. Atmos.*, 112(20), doi:10.1029/2006JD008298, 2007.
- 681 Sturm, K., Hoffmann, G., Langmann, B. and Stichler, W.: Simulation of $\delta^{18}\text{O}$ in precipitation by
682 the regional circulation model REMO iso, *Hydrol. Process.*, 19(17), 3425–3444,
683 doi:10.1002/hyp.5979, 2005.
- 684 Treydte, K., Boda, S., Graf Pannatier, E., Fonti, P., Frank, D., Ullrich, B., Saurer, M., Siegwolf,
685 R., Battipaglia, G., Werner, W. and Gessler, A.: Seasonal transfer of oxygen isotopes from
686 precipitation and soil to the tree ring: Source water versus needle water enrichment, *New Phytol.*,
687 202(3), 772–783, doi:10.1111/nph.12741, 2014.
- 688 Viereck, L. A. and Johnston, W. F.: *Picea mariana* (Mill.) B. S. P., in *Silvics of North America:*
689 *1. Conifers; 2. Hardwoods.*, edited by R. M. Burns and B. H. Honkala, pp. 443–464, US.
690 Department of Agriculture, Forest Service, Washington, DC., 1990.
- 691 Wernicke, J., Griebinger, J., Hochreuther, P. and Braüning, A.: Variability of summer humidity
692 during the past 800 years on the eastern Tibetan Plateau inferred from $\delta^{18}\text{O}$ of tree-ring
693 cellulose., *Clim. Past*, 11, 327–337, doi:10.5194/cp-11-327-2015, 2015.
- 694 Wershaw, R. L., Friedman, I. and Heller, S. J.: Hydrogen isotope fractionation in water passing
695 through trees, in *Advances in Organic Geochemistry*, edited by F. Hobson and M. Speers, pp. 55–
696 67, New York, Pergamon., 1966.
- 697 Yakir, D. and DeNiro, M. J.: Oxygen and Hydrogen Isotope Fractionation during Cellulose
698 Metabolism in *Lemna gibba* L., *Plant Physiol.*, 93(1), 325–332, doi:10.1104/pp.93.1.325, 1990.



699

Tables and Figures

700

701 **Table 1** Definition of sensitive parameters. The posterior medians and 90% confidence intervals
 702 are also shown.

703

Parameter	Definition	Unit	Parameter type (prior range)	Values with 90% posterior confidence intervals
f_0	Dampening factor	NA	Calibrated (0.3 to 0.5)	0.36 [0.31; 0.46] (Arg.) 0.41 [0.32; 0.48] (Q.)
ε_0	Biochemical fractionation	‰	Calibrated (24 to 30)	29.99 [29.93; 30] (Arg.) 26.81 [24.74; 28.04] (Q.)
ε_k	Kinetic fractionation	‰	Calibrated (10 to 30)	28.86 [18.25; 29.96] (Arg.) 17.20 [11.16; 26.34] (Q.)
a	Temperature dependence of $\delta^{18}O_P$	NA	Calibrated (0.2 to 0.5 for Arg. and 0 to 0.38 for Q.)	0.50 [0.49; 0.50] (Arg.) 0.31 [0.25; 0.37] (Q.)
b	Precipitation dependence of $\delta^{18}O_P$	NA	Calibrated (-0.3 to 0 for Arg. and -0.39 to 0 for Q.)	-0.009 [-0.15; 0] (Arg.) -0.22 [-0.35; -0.14] (Q.)
c	Intercept of $\delta^{18}O_P$	‰	Fixed	-10.0 (Arg.) -11.9 (Q.)

704

705

706

707 **Table 2** Climate input data for all tested simulations

708

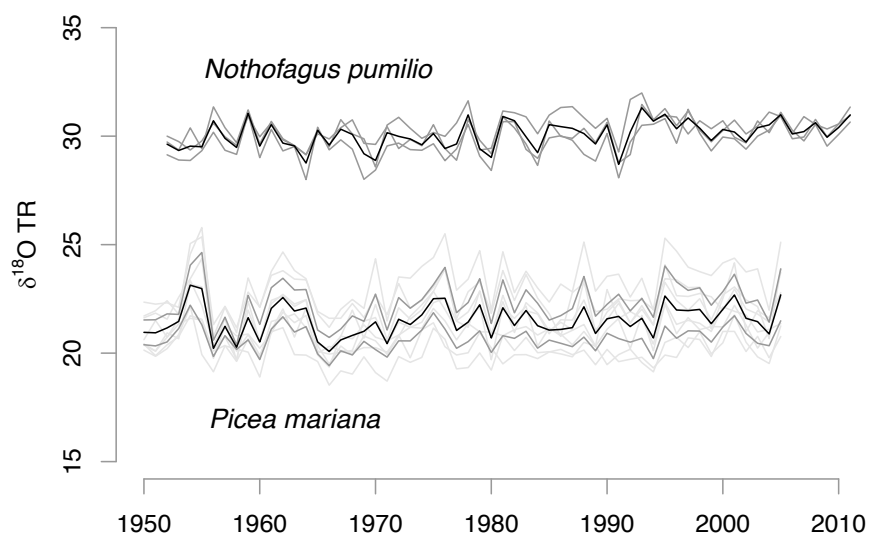
	Daily Tmin and Tmax	Daily P	Daily $\delta^{18}O_P$	CO ₂
Configuration 1	Canadian database/ NOAA-CIRES dataset		Linear regression	Mauna
Configuration 2	Canadian database / NOAA-CIRES dataset	MUGCM data		Loa station
Configuration 3	LMDZ-NCEP20 data			

709

710



711 **Figure 1** Tree-ring $\delta^{18}\text{O}$ time series (‰) at the three sites in Argentina (NUB, ALM and CHA in
712 dark grey) and two sites in Quebec (L01 and L20 in dark grey; single trees in light grey). The
713 bold black lines are the averaged values. The mean inter-site correlation coefficients are
714 $r = 0.60$, $p < 0.05$ and $r = 0.80$, $p < 0.01$ in the South and North American sites, respectively.
715

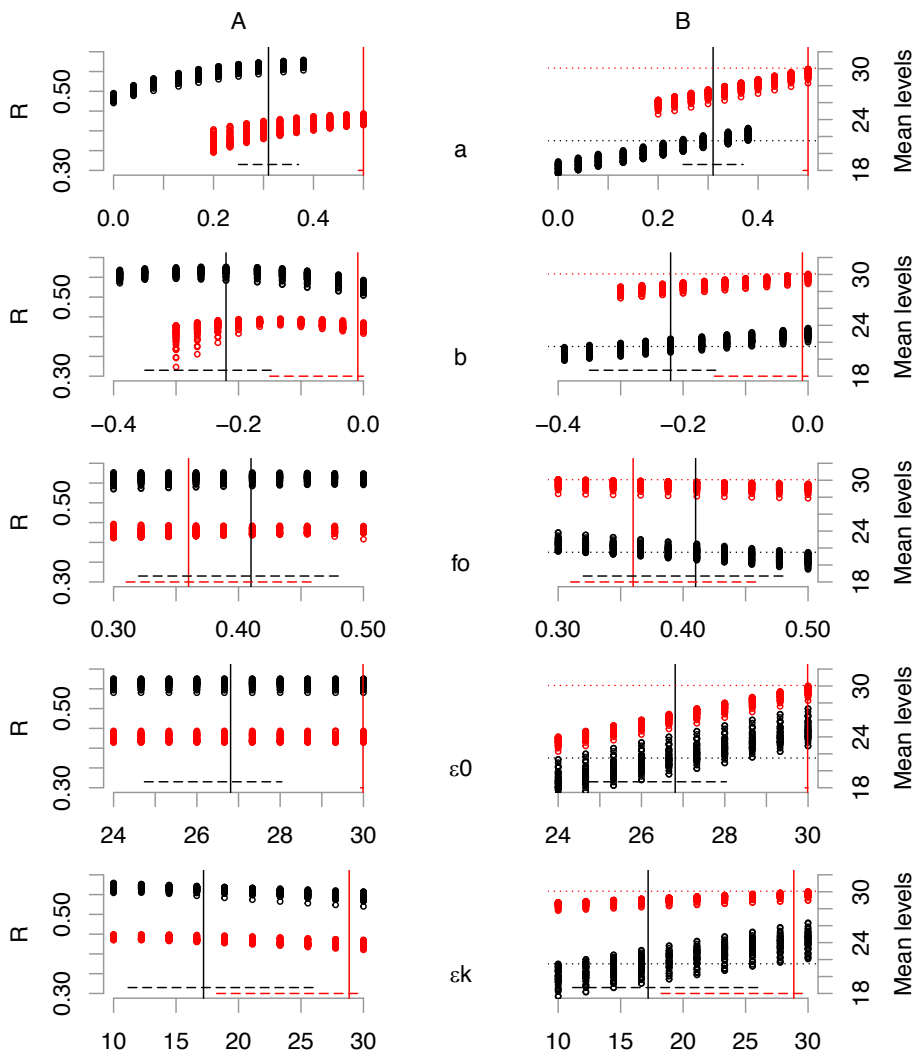


716

717



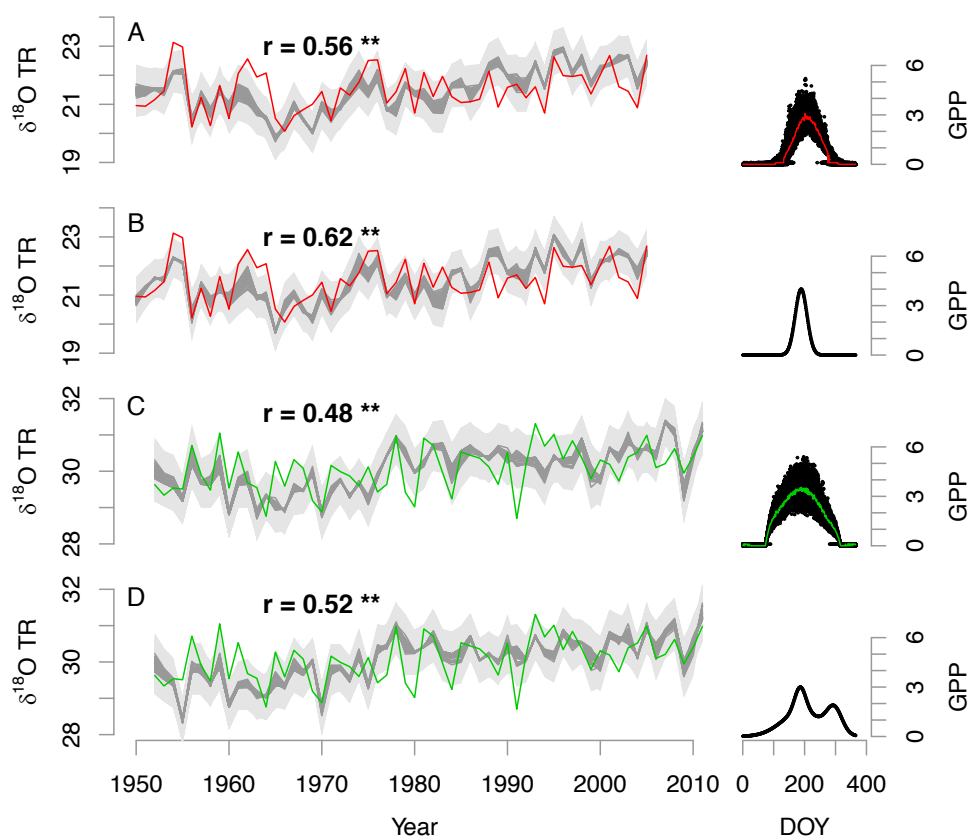
718 **Figure 2** Dependence of the correlation coefficients between observed and simulated $\delta^{18}\text{O}_{\text{TR}}$
 719 series (panels A), and of the mean simulated $\delta^{18}\text{O}_{\text{TR}}$ levels (‰) (panels B) as a function of the
 720 range of calibrated parameters a , b , f_o , ε_0 and ε_k for the 50 simulations performed. In black are the
 721 tests with the sites from Quebec and in red the ones with the Argentinean sites. The vertical lines
 722 are the values of a plausible block of parameters retained in the MCMC optimization. The
 723 horizontal dashed lines are their respective 90% confidence interval calculated with 50
 724 simulations (see Table 1). The horizontal dot lines in panel B are the mean values of the observed
 725 $\delta^{18}\text{O}_{\text{TR}}$.



726



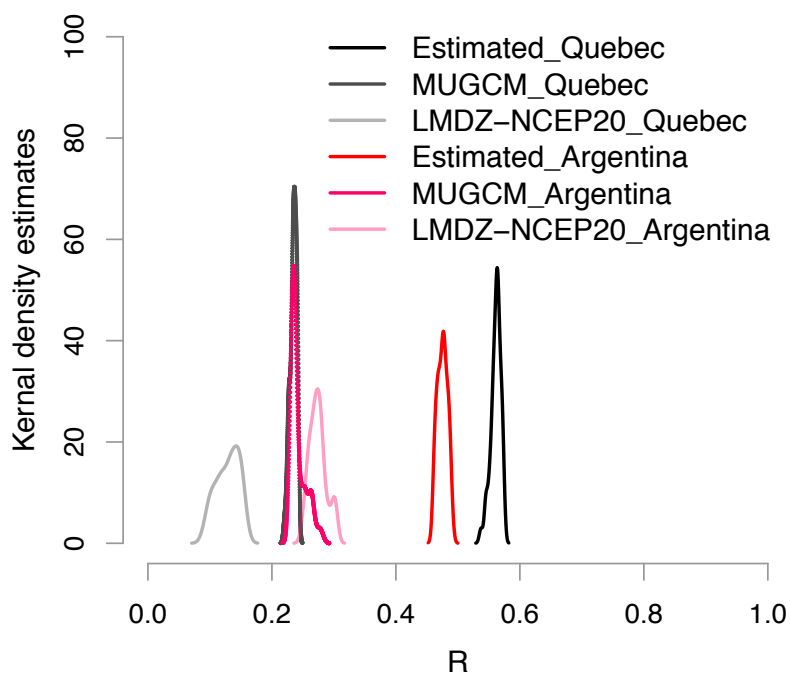
727 **Figure 3** Comparison between observed (red or green) and simulated (grey) $\delta^{18}\text{O}_{\text{TR}}$ chronologies
728 in Quebec (A and B) and Argentina (C and D), respectively, using GPP (in $\text{gC}\cdot\text{m}^{-2}\cdot\text{day}^{-1}$)
729 simulated by MAIDENiso (A and C) or synthesized for maximizing correlations (B and D). The
730 simulations are based on estimated $\delta^{18}\text{O}_{\text{P}}$ series. The 50 different simulations inferred from the
731 Markov Chain Monte Carlo (MCMC) chains are in dark grey. The ± 1 root mean square error
732 (RMSE) range is represented in light grey. The mean correlation coefficients are significant at
733 99% level (**).



734
735



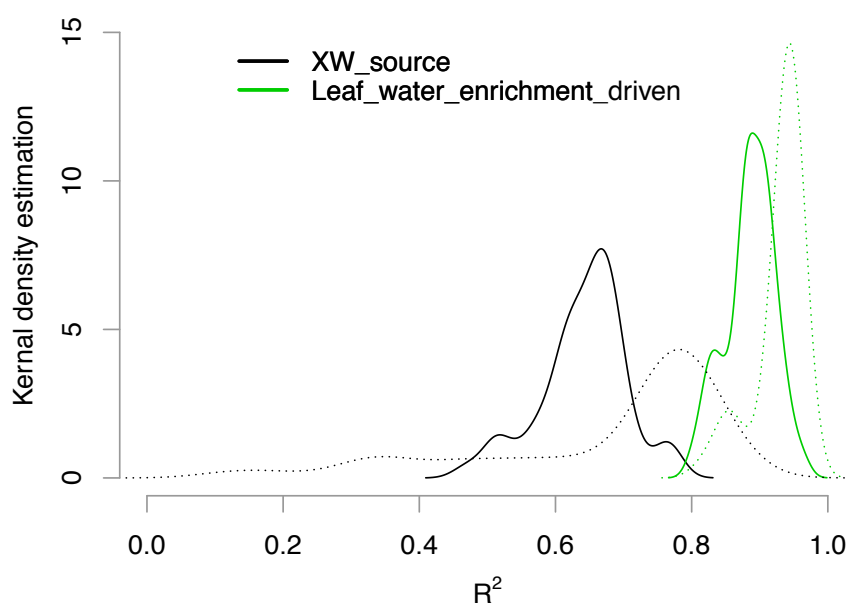
736 **Figure 4** Comparison of the densities of probability of the coefficient of correlation (R) between
737 observed and simulated $\delta^{18}\text{O}_{\text{TR}}$ chronologies in Quebec and Argentina when the simulations are
738 based on $\delta^{18}\text{O}_{\text{P}}$ series estimated by the regression model or from the MUGCM and LMDZ-
739 NCEP20 models.
740



741
742



743 **Figure 5** Density distributions of the coefficients of determination (R^2) between the reference
744 simulations and the: 1) XW_source experiment simulation ($\delta^{18}\text{O}_V$ and h_{air} set as constant, black)
745 and, 2) Leaf_water_enrichment_driven experiment simulation ($\delta^{18}\text{O}_{\text{XW}}$ set as constant, green) in
746 Quebec (bold line) and Argentina (dashed line).



747
748
749